



Li₄Ti₅O₁₂ prepared by a modified citric acid sol–gel method for lithium-ion battery

Chunming Zhang^a, Yaoyao Zhang^b, Jin Wang^a, Dan Wang^a, Dannong He^{a,b,*}, Yongyao Xia^{c,**}

^aNational Engineering Research Center for Nanotechnology, No. 28 East Jiangchuan Road, Shanghai 200241, PR China

^bSchool of Material Science and Engineering, Shanghai Jiaotong University, No. 880 Dongchuan Road, Shanghai 200240, PR China

^cDepartment of Chemistry and Shanghai Key Laboratory of Molecular Catalysis and Innovative Materials, Institute of New Energy, Fudan University, Shanghai 200433, PR China

HIGHLIGHTS

- An enhanced chelating agent scheme for uniformly distributed products.
- Ethylene diamine tetraacetic acid (EDTA) and citric acid (CA) as the bi-components chelating agent.
- The bi-components chelating agent to improve the particles dispersion and decrease the particle size.
- Nano-scale Li₄Ti₅O₁₂ oxides show superior electrochemical performance and cycle life.
- The bi-components chelating agent scheme is robust and efficient.

ARTICLE INFO

Article history:

Received 24 October 2012

Received in revised form

18 January 2013

Accepted 21 January 2013

Available online 28 January 2013

Keywords:

Li₄Ti₅O₁₂

EDTA–CA

Sol–gel method

Anode material

Lithium-ion battery

ABSTRACT

Li₄Ti₅O₁₂ was synthesized by a modified and facile sol–gel method with ethylene diamine tetraacetic acid (EDTA) and citric acid (CA) as a bi-components chelating agent. The raw precursor and powders further calcined at various temperatures and holding time were characterized by XRD, FT-IR, TG, BET and SEM. Nano-scale Li₄Ti₅O₁₂ oxides, with a high phase purity and good stoichiometry, can be obtained at a calcination temperature of 750 °C and higher. The Li₄Ti₅O₁₂ nanoparticle shows a network morphology with high dispersion, which reached a capacity of 164 and 108 mAh g⁻¹ at 1C and 10C discharge rate, respectively. The result of the cycling performance shows a high capacity maintenance ratio of 97% at 1C and 25 °C after 1000 cycles. Electrochemical lithium intercalation/extraction performance is also evaluated by electrochemical impedance spectroscopy (EIS) and cyclic voltammetry (CV) at room temperature.

© 2013 Elsevier B.V. All rights reserved.

1. Introduction

As a rechargeable energy-storing device and conversion technology with no emissions, Li-ion battery has been wildly used in portable electronic devices, communication facilities, electric vehicles (EV, HEV and PHEV) and stationary energy storage systems [1–5]. The conventional Li-ion batteries typically use graphite/carbon-based anode materials. However, a stable solid electrolyte interface (SEI) film formed on the surface of graphite/carbon particles and volume expansion/contraction

during Li-ion intercalation/extraction could possibly cause serious safety issues. Furthermore, graphite/carbon-based anodes are also suffering from greater energy loss and poor high-rate discharge/charge performance [6–8].

Nowadays, spinel Li₄Ti₅O₁₂ oxide is developed as a promising alternative anode material for solid, liquid and gel Li-ion batteries because of its excellent Li-ion intercalation/extraction reversibility with negligible volume change. Moreover, it exhibits a flat discharge platform at ~1.55 V (vs. Li) which is higher than the reduction potential of the most organic electrolytes (~0.8 V), thus avoiding SEI film formation on the surface of Li₄Ti₅O₁₂ particles [9,10] and ensuring a longer cycling life and better safety of the battery [11–17]. Although Li₄Ti₅O₁₂ has a theoretical specific capacity of 175 mAh g⁻¹, its high charge/discharge rate capabilities are relatively low because of a large polarization due to the poor electrical conductivity and ultra-slow Li-ion diffusion [18,19]. Many approaches have been

* Corresponding author. National Engineering Research Center for Nanotechnology, No. 28 East Jiangchuan Road, Shanghai 200241, PR China. Tel.: +86 21 34291286; fax: +86 21 34291121.

** Corresponding author. Tel./fax: +86 21 51630318.

E-mail addresses: hdnbill@sh163.net (D. He), yyxia@fudan.edu.cn (Y. Xia).

developed to overcome these shortcomings and then improve the battery performance. One effective way is reducing the particle size which can shorten the Li-ion diffusion path and provide extended contact area between the electrode and electrolyte, consequently, improving Li-ion intercalation kinetics [20–22]. The other way is improving the electrical conductivity by surface modification and cation ion doping. Various kinds of high conductive phase, such as oxides [23,24], metals [25–27] and carbon materials [28–31], has been introduced for surface coatings to improve the surface electronic conductivity of the resultant materials. The bulk electronic conductivity can be enhanced by incorporating cations of conventional, transition and rare earth metals [32–35] and anions of F^- [36] and Br^- [37] into the framework of $Li_4Ti_5O_{12}$ to improve its imperfect structure. In these ways, the performance of the anode at a high charge/discharge rate has been exploited.

However, $Li_4Ti_5O_{12}$ powders were mainly prepared by a solid-state reaction of lithium and titanium salts at higher calcination temperatures between 800 and 1100 °C [38–40], which would introduce several disadvantages, including low homogeneity, irregular morphology, large particle size and long calcination time. On the other hand, a sol–gel method, which could obtain decentralized and decreased particles in a relatively low calcination temperature, has been widely developed for the synthesis of $Li_4Ti_5O_{12}$ materials in Li-ion battery's application. In our previous work [41], carbon-coated $Li_4Ti_5O_{12}$ has been in situ synthesized by citric acid (CA) sol–gel method. Experiments show that CA was not only used as a chelating agent and carbon resource, but also as the dispersant and stabilizing agent to prevent the nanoparticles aggregating. However, the electrochemical performance has been only improved to a certain extent, due to the reaction-formed $Li_4Ti_5O_{12}$ particles are nonuniform in size and distribution.

In the present work, nano-sized $Li_4Ti_5O_{12}$ is prepared for the first time by a modified sol–gel route using ethylenediaminetetraacetic acid (EDTA) and CA as a bi-components chelating agent with different molar ratio of Li to Ti ions, calcination temperatures and holding time. Influences of the microstructure and particle size of the products on the electrochemical properties are investigated. The stability of the $Li_4Ti_5O_{12}$ electrode is also studied.

2. Experimental

2.1. Powder synthesis

$Li_4Ti_5O_{12}$ was synthesized by the sol–gel method using the standard combined EDTA–citrate as a chelating agent, as shown in Fig. 1. Stoichiometric amounts of tetrabutyl titanate [$Ti(C_4H_9O)_4$, TBT] and Li_2CO_3 was dissolved in ethanol– HNO_3 preblended solution in the volume ratio of TBT: ethanol: HNO_3 of 1:12:0.5. The necessary amount of EDTA and CA, which were pre-dissolved in ammonia, was then gradually dropped into the mixed metal ion solution (the mole ratio of total metal ions to EDTA and to CA is 1:1:2). $NH_3 \cdot H_2O$ was used to adjust the pH value of the solution to the aimed value, and then the mixed solution was slowly stirred for 12 h. And then the solution finally turned into a transparent gel after drying at 80 °C. The resulting gelatin was heat-treated in an electric oven at 250 °C over 6 h to extract out excess ethanol and yield a solid organic $Li_4Ti_5O_{12}$ precursor. The solidified precursor was first pretreated by planetary ball milling (Ntu Instrument Factory, Nanjing, China) and then calcined under open air at 700–800 °C for different times to obtain final powders.

2.2. Electrode fabrication

The electrochemical cells consisted of Li metal as the anode, $Li_4Ti_5O_{12}$ based composite as the cathode and 1 M solution of $LiPF_6$

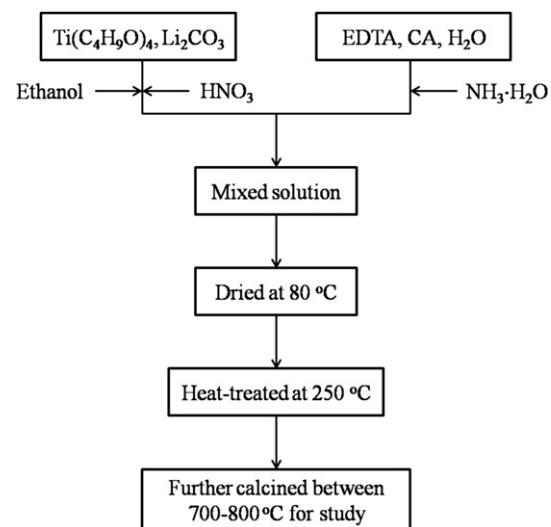


Fig. 1. A flow-chart for the synthesis of $Li_4Ti_5O_{12}$ via the EDTA–CA sol–gel process.

in ethylene carbonate (EC) and dimethyl carbonate (DMC, EC:DMC = 1:1, v/v). Microporous polypropylene sheet (Celgard, 2400) was used as the separator. The working electrode was fabricated by mixing 85:10:5 (w/w) ratio of $Li_4Ti_5O_{12}$ active material, a carbon (acetylene black) electronic conductor and polyvinylidene fluoride (PVDF) binder, respectively, using N-methyl-2-pyrrolidone (NMP) as the solvent. The slurry was then coated on the copper foil (~10 μm) current collector and dried under vacuum at 120 °C for 12 h. The cells were assembled in a glove box filled with pure argon.

2.3. Basic characterization

The amount of the $Li_4Ti_5O_{12}$ precursors was measured by a mal gravimetric (TG) method using a TG-DSC analyzer (Model NETZSCH STA449C, Germany) from room temperature to 800 °C at a heating rate of 10 °C min⁻¹ in air. The crystal structures of the synthesized powders were examined by X-ray diffraction (XRD) using a Bruker D8 advance diffractometer with nickel filtered Cu $\kappa\alpha$ radiation ($\lambda = 1.5418 \text{ \AA}$) over the 2θ range from 10° to 80°. Fourier transformed infrared analysis (FT-IR, Nicolet 170SX, American) was performed on KBr-supported samples using a GX spectrometer. The particle morphology was observed using JEOL-6930 scanning electron microscopy (SEM) and JEOL-2100F transmission electronic microscopy (TEM). The specific surface area of the samples was determined by N_2 adsorption using a 3H-2000 specific surface area instrument (Beishide Instrument-ST Co., Ltd., Beijing, China). The samples were treated at 200 °C for 3–5 h in a vacuum to remove the surface adsorbed species.

2.4. Electrochemical characterization

The charge/discharge characteristics of the cells were performed over the potential range between 1.0 and 3.0 V using a NEWARE BTS 5 V-10 mA computer-controlled Galvanostat (Shenzhen, China) at different rates of 0.5–10 C at room temperature. Electrochemical impedance spectroscopy (EIS) was carried out using CHI660B electrochemical workstation (Shanghai Chenhua Instrument Co. Ltd., China) in the frequency range from 0.1 Hz to 1 MHz. Cyclic voltammetry tests were performed by a CHI660B electrochemical workstation over the potential range of 1.0–3.0 V vs. Li^+/Li at the scanning rate of 0.5 mV s⁻¹.

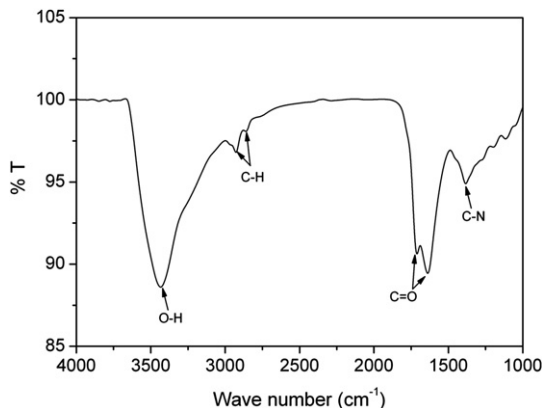


Fig. 2. FT-IR spectra of $\text{Li}_4\text{Ti}_5\text{O}_{12}$ precursor pre-treated at $250\text{ }^\circ\text{C}$ for 12 h in an electrical oven.

3. Results and discussion

3.1. Powder characterization

The EDTA–CA sol–gel method has been extensively used for fabrication of electrode materials in solid oxide fuel cells [42,43], and the final products exhibit excellent electrochemical performance. It is well known that EDTA usually forms four or six five-membered rings with most metal ions while the chelating reaction is fast, complete and in one single step, and the product is stable and disperse; CA is one of the most applied chelating agents in the Pechini method. Moreover, the presence of hydroxyl groups in CA's structure makes the polymerization reaction possible to happen between CAs or between CA and EDTA. Zhou et al. [42] also demonstrated this EDTA–CA–metal complexing reaction is the non-ion selective processes through a series of experiments. Thus, EDTA combined CA as the bi-components chelating agent could effectively eliminate the difference between various metal ions and help the molecule level mixing of the metal ions in the precursor.

To demonstrate whether the EDTA–CA sol–gel method is a versatile process for the synthesis of $\text{Li}_4\text{Ti}_5\text{O}_{12}$, the precursor and final $\text{Li}_4\text{Ti}_5\text{O}_{12}$ product were characterized by FT-IR and SEM. As shown in Fig. 2, there were six absorption bands appeared between 1000 and 4000 cm^{-1} for the precursor. The band around 3430 cm^{-1} is assigned to the stretching vibration of O–H originated probably from the humidity effect of KBr medium. Moreover, other absorption bands such as around 1380 cm^{-1} , 1600 – 1720 cm^{-1} and 2850 – 3000 cm^{-1} , which are assigned to the stretching vibrations of the C–N band, C=O band and C–H band, respectively. All of them can be used as the dispersant due to the large amounts of gases were emitted in the calcination process. The SEM and TEM images of the obtained powders prepared by further calcinations at $750\text{ }^\circ\text{C}$ for 5 h in air are presented in Fig. 3. As shown in Fig. 3A and B all the $\text{Li}_4\text{Ti}_5\text{O}_{12}$ particles formed a uniform distribution of three-dimensional space network structure with the particle size of 200 – 500 nm . Fig. 3C and D are the high resolution transmission electron microscopy (HRTEM) and selected-area electron diffraction (SAED) images and the results show that the $\text{Li}_4\text{Ti}_5\text{O}_{12}$ particles are excellent crystallinity. It suggests that the combustion process of the chelating agent can create abundant pore space and the fine size of $\text{Li}_4\text{Ti}_5\text{O}_{12}$ particles at a relatively low calcination temperature.

Fig. 4 shows the TG curve of $\text{Li}_4\text{Ti}_5\text{O}_{12}$ precursor performed in a flowing air atmosphere between 40 and $800\text{ }^\circ\text{C}$. Three evident steps of weight loss were presented in the TG curve. The first step is the evaporation of water and partial organic at the temperature range from 40 to $280\text{ }^\circ\text{C}$. The second step is obviously due to the liberation of the free EDTA, CA, NH_4NO_3 and the complex compounds to successive combustion around 280 and $500\text{ }^\circ\text{C}$. The weight loss is about 89% in this temperature range. Meanwhile, the probable products of CO_2 , NO_x , N_2 and vapor, which were produced from this combustion process, could inhibit the grain growth of nanoparticles and prevent the subsequent aggregation significantly. This process depicts the decomposition of the organics and the elementary formation of $\text{Li}_4\text{Ti}_5\text{O}_{12}$ phase. The third step in the temperature range between 500 and $800\text{ }^\circ\text{C}$ shows no weight loss. The result confirms that the phase-change reaction and formation of $\text{Li}_4\text{Ti}_5\text{O}_{12}$ crystalline phase may occupy during this temperature range. Thus, pure phase nanocrystalline $\text{Li}_4\text{Ti}_5\text{O}_{12}$ may be obtained by controlling the sintering temperature at least above $500\text{ }^\circ\text{C}$.

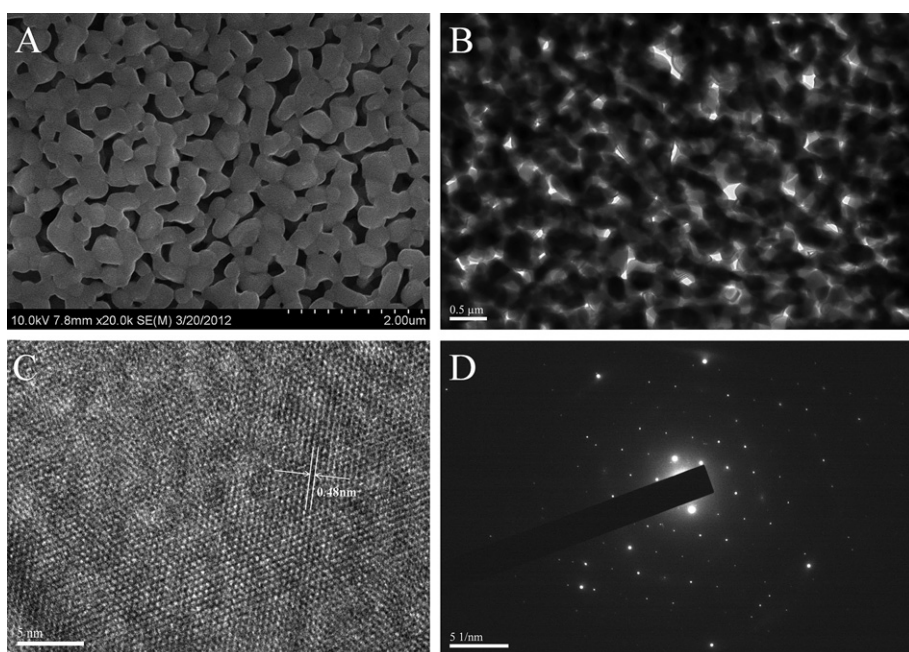


Fig. 3. (A) SEM and (B) TEM (C) HRTEM (D) SAED images of the obtained $\text{Li}_4\text{Ti}_5\text{O}_{12}$ powder prepared by EDTA–CA sol–gel process after calcined at $750\text{ }^\circ\text{C}$ for 5 h in air.

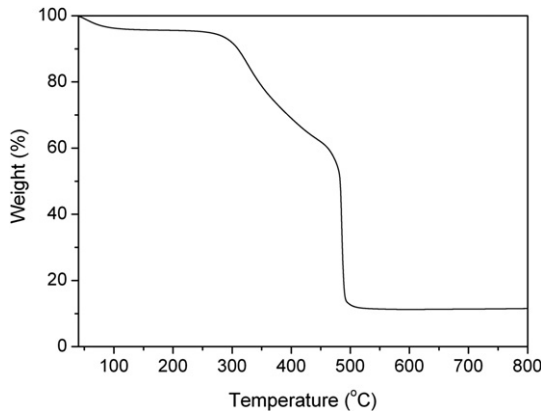


Fig. 4. TG curve of $\text{Li}_4\text{Ti}_5\text{O}_{12}$ precursor pre-treated at 250 °C for 12 h in an electrical oven.

In order to obtain a pure phase $\text{Li}_4\text{Ti}_5\text{O}_{12}$, the conditions of Li/Ti ratio and sintering temperature were both discussed. As shown in Fig. 5A, pure phase $\text{Li}_4\text{Ti}_5\text{O}_{12}$ was obtained only in the Li/Ti ratio equals 4.2:5 after the calcination at 750 °C for 5 h. The rutile TiO_2 was observed when the ratio was less than above values, it indicates some loss of lithium during the high temperature calcination. And the monoclinic phase Li_2TiO_3 was also observed when the ratio was higher than the one. Both the rutile TiO_2 and Li_2TiO_3 could reduce the electrochemical performance of the materials. Fig. 5B shows $\text{Li}_4\text{Ti}_5\text{O}_{12}$ precursor calcined at different temperatures and hours in air after pre-heated at 250 °C for 12 h. After calcining the precursor between 250 and 750 °C, the diffraction peaks of $\text{Li}_4\text{Ti}_5\text{O}_{12}$ gradually sharpened with the increasing of temperature. It indicates an increase of crystallinity of the oxide with temperatures rising. The average crystalline sizes and the specific surface area of the $\text{Li}_4\text{Ti}_5\text{O}_{12}$ oxides calcined at various temperatures and holding time are listed in Table 1, while the average crystalline sizes were calculated from XRD line broadening with Scherer's equation. With the increase of calcination temperature and holding time, the particle size increased while the specific surface area decreased obviously.

Fig. 6A–F show the SEM morphologies of $\text{Li}_4\text{Ti}_5\text{O}_{12}$ oxides prepared by further calcination of the middle product (the precursor was pre-treated by ball milling for 10 h) at various temperatures between 750 and 800 °C for different hours in air atmosphere. It can be seen that the ball milling could effectively reduce the particle size from the original 200–500 to 150–400 nm for the sample calcined at 750 °C for 5 h. In addition, the surface of the $\text{Li}_4\text{Ti}_5\text{O}_{12}$ particles is relatively smooth and evenly dispersed in most of the display area after the ball milling treatment. It suggests that the ball milling method can decrease the particle size and prevent the aggregation. And it was found the particle size of $\text{Li}_4\text{Ti}_5\text{O}_{12}$ increased with the increase of calcination temperature and holding time. The oxides calcined at 750 °C show a much porous morphological structure than the one calcined at 800 °C, while the large particles with main sizes of 1 μm was observed in the sample calcined at 800 °C for 15 h. Based on the previous results [21], the smaller particle size of the $\text{Li}_4\text{Ti}_5\text{O}_{12}$ could introduce more active sites for the charge transfer processes and reduce the diffusion resistance of Li^+ and electron, thus the further promotion of the battery's electrochemical performance could be expected.

3.2. Electrochemical characterization

To demonstrate whether the calcination time at 750 °C for 5 h is the optimized conditions, some electrochemical tests were carried. Fig. 7(A–F) show the first discharge/charge curves of the cells with

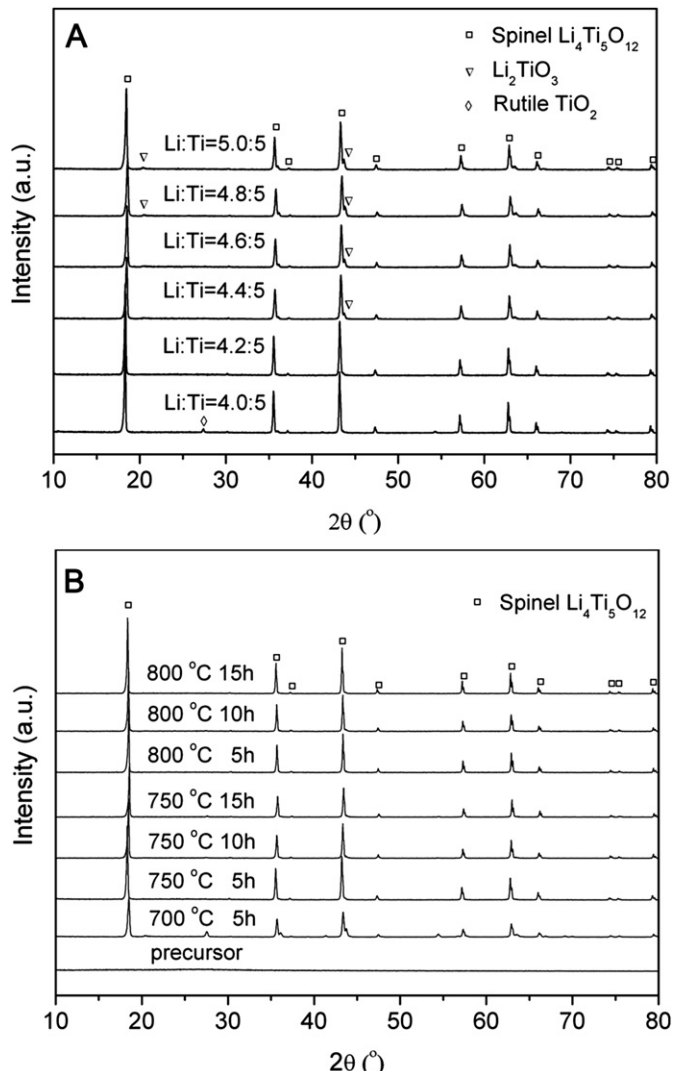


Fig. 5. X-ray diffraction patterns of $\text{Li}_4\text{Ti}_5\text{O}_{12}$ prepared by the EDTA–CA sol–gel method (A) with the ratios of Li/Ti equal 4.0–5.0:5.0 and calcined further at 750 °C for 5 h; (B) Calcined at various temperatures between 700 and 800 °C, and holding time between 5 and 15 h.

various electrodes at the rate between 0.5 and 40C over the potential range of 1.0–3.0 V, in which anode material was prepared by EDTA–CA sol–gel method with calcination temperatures between 750 and 800 °C and holding time between 5 and 15 h. At a discharge rate of 0.5C, high capacities of around 175 mAh g⁻¹ were obtained for all the samples due to the enough diffusion time for both Li^+ and electron at this low current rate. It also clearly shows that the difference values of the capabilities between 0.5 and 40C rates for 750 °C calcined samples were significantly lower than the 800 °C calcined ones at each holding time. It indicates that the differences between the reversible capacities of them become even

Table 1

Surface areas and crystalline sizes of the $\text{Li}_4\text{Ti}_5\text{O}_{12}$ prepared by the EDTA–CA sol–gel method calcined further at various temperatures and holding time.

Temperature (°C)	750			800		
	5	10	15	5	10	15
Surface area (m ² g ⁻¹)	4.34	4.30	3.96	3.09	2.89	1.86
Crystalline size (nm)	57.75	67.39	80.89	83.89	88.05	95.88

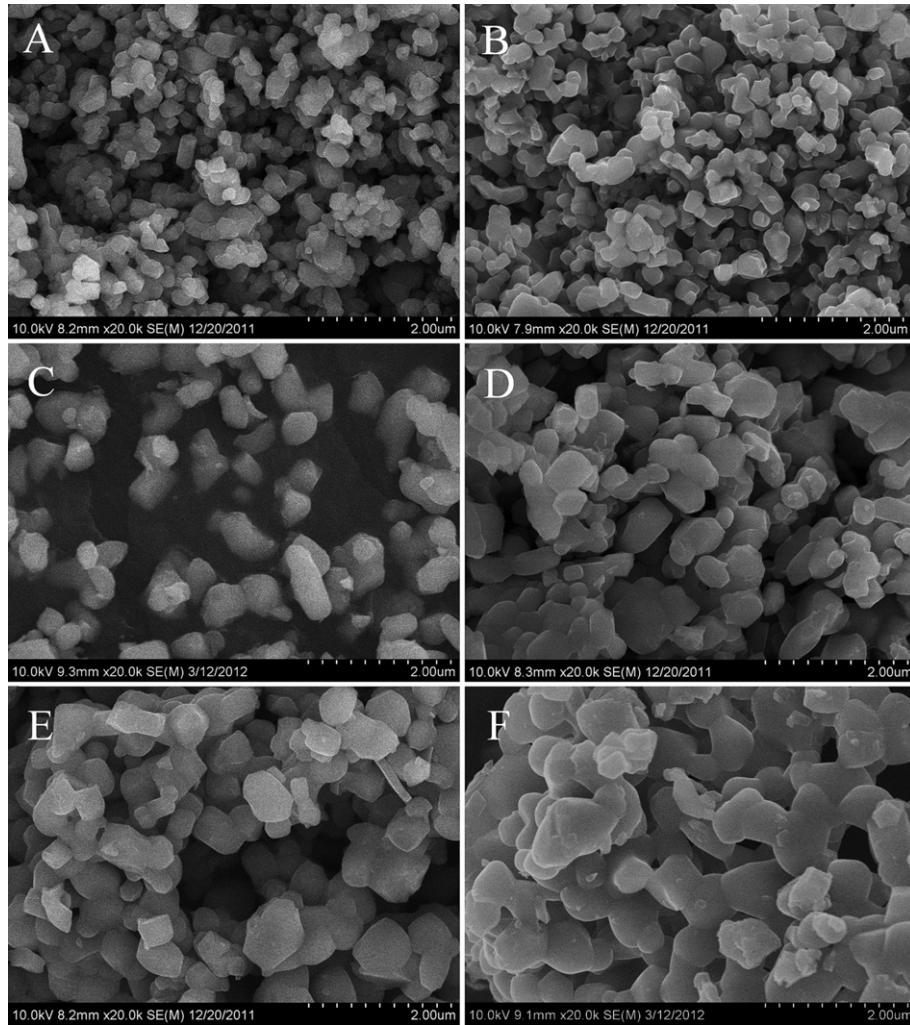


Fig. 6. SEM photos of $\text{Li}_4\text{Ti}_5\text{O}_{12}$ prepared by the EDTA-CA sol–gel method calcined further at 750 °C for (A) 5 h; (B) 10 h; (C) 15 h; and 800 °C for (D) 5 h; (E) 10 h; (F) 15 h.

more obvious with increasing the charge/discharge current rate. As shown in Fig. 7A, the first discharge capacities for the cell with the 750 °C for 5 h calcined $\text{Li}_4\text{Ti}_5\text{O}_{12}$ sample reached 181, 164, 156, 139, 108, 76 and 49 mAh g^{-1} at 0.5C, 1C, 2C, 5C, 10C, 20C and 40C, respectively. It displays the greatest 40C capability of all the samples. This result suggests that the smallest crystalline size of $\text{Li}_4\text{Ti}_5\text{O}_{12}$ electrode material had the largest Li ion extraction/insertion and electronic diffusivity at the high rate. Consequently, the discharge–charge capacities at the high current rate decreased with the increase of $\text{Li}_4\text{Ti}_5\text{O}_{12}$ precursor calcination temperature and holding time.

The cycling behavior of the cell with the 750 °C for 5 h calcined $\text{Li}_4\text{Ti}_5\text{O}_{12}$ electrode was further carried out, which was progressively charged and discharged in series stages at the charge/discharge rate range of 0.5C to 40C. For each stage, the process was taken with 100 cycles. As shown in Fig. 8A, the stable discharged capacities were observed at each stage. After 100 charge/discharge cycles, the discharge capacity was 162 mAh g^{-1} at 1C, which was less than 1.52% discharge capacity loss. It suggests good stability of the synthesized nano $\text{Li}_4\text{Ti}_5\text{O}_{12}$ from the EDTA-CA sol–gel method for rechargeable lithium battery. As compared to other literature using CA or modified CA sol–gel method [41,44], this proposed method has been proven feasible and effective for the preparation of $\text{Li}_4\text{Ti}_5\text{O}_{12}$ material due to its higher

and more stable electrochemical performance for all discharge/charge rates. It is a widely recognized fact that the $\text{Li}_4\text{Ti}_5\text{O}_{12}$ electrode shows an irreversible capacity at the first discharge/charge cycle. The capacity loss at the early few cycles was also observed by many other researchers [28,45]. Three explanations were provided: first, the irreversible insertion of Li into electroconductive carbon particles due to the higher cutoff voltage ($\text{Li}_4\text{Ti}_5\text{O}_{12}$ is 1.0 V and carbon is 0.02 V, vs. Li/Li^+); second, the $\text{Li}_4\text{Ti}_5\text{O}_{12}$ electrode with high BET surface area may have more active sites for the charge transfer processes and further reduce the diffusion resistance of Li-ion and electron; third, the possible decomposition of the electrolyte due to the dissolution of some impurities from the $\text{Li}_4\text{Ti}_5\text{O}_{12}$ electrode into the organic electrolyte solution. At 0.5C rate, the above reasons can explain the capacity loss at the early few cycles. However, the reasons of capacity loss at high discharge/charge rates in Fig. 8A are different. This may be ascribed to the lithium insertion in the bulk $\text{Li}_4\text{Ti}_5\text{O}_{12}$ can't completely deintercalated from (16c) sites when discharge rate is suddenly changed from low rate to high rate. The lithium ion would be slowly released in the subsequent process of charging and discharging. Therefore, the discharge capacities of $\text{Li}_4\text{Ti}_5\text{O}_{12}$ at each higher rate are expressed stably with an increased number of cyclings. However, the capacity loss at 40C rate was larger than the others.

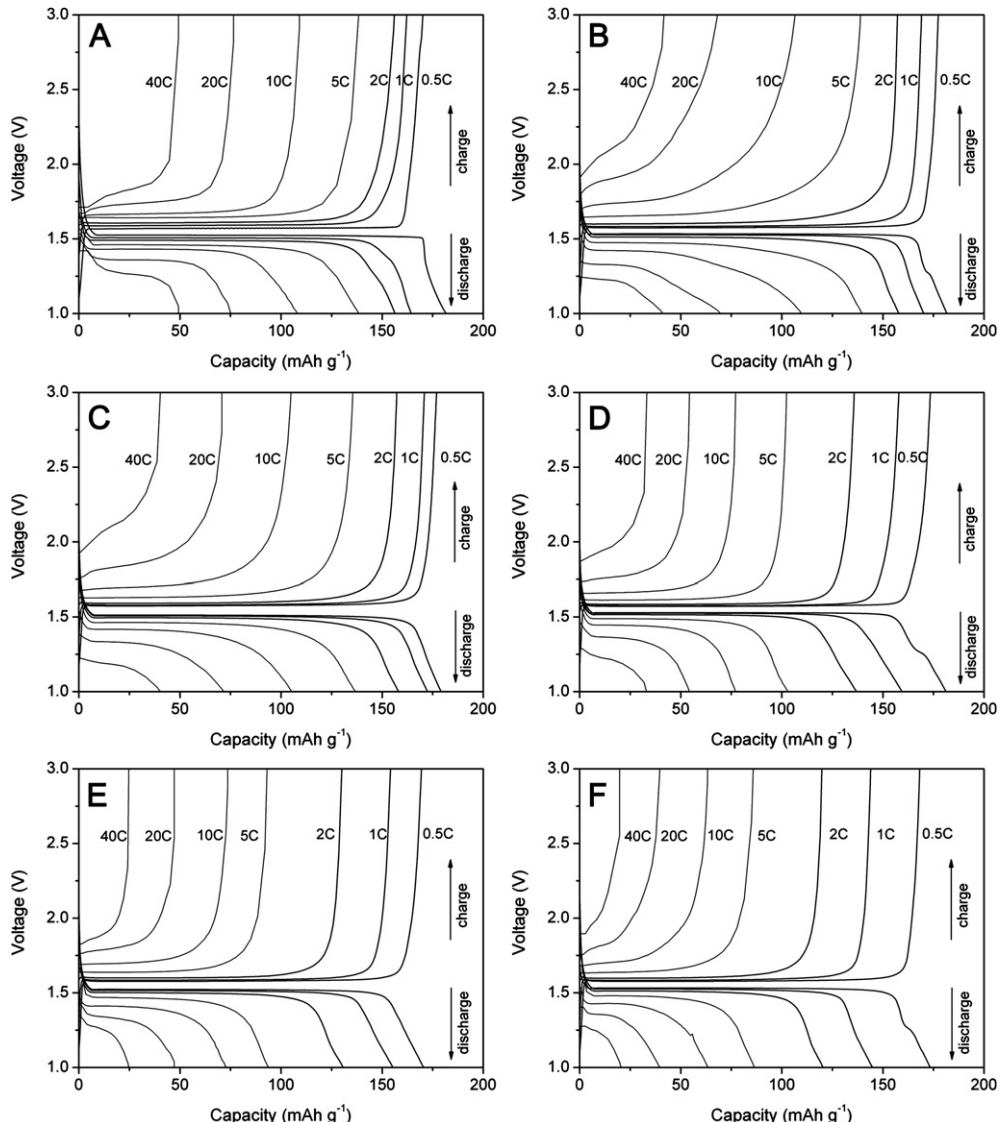


Fig. 7. A comparison of the discharge and charge curves of $\text{Li}_4\text{Ti}_5\text{O}_{12}$ oxides from 1 to 3 V at different rates, prepared by the EDTA–CA sol–gel method and further calcined at 750 $^{\circ}\text{C}$ for (A) 5 h; (B) 10 h; (C) 15 h; and 800 $^{\circ}\text{C}$ for (D) 5 h; (E) 10 h; (F) 15 h.

To demonstrate whether the anode powder was loosened from the current collector of the copper film during the operation, the testing current rate was then returned to 1C. As shown in Fig. 8B, the reversible capacity still stayed in $\sim 162 \text{ mAh g}^{-1}$. This result confirms that the adhesion of the active materials to the current collector was very well. The probable reason is the reunion was happening between parts of the nanoparticles during the high rate charge/discharge process and long time operation, and then the electrochemical performance was reduced at high discharge rate. Furthermore, the sample shows very long-term operational stability at 1C discharge rate. After 1000 cycles, the discharge capacity was still as high as 160 mAh g^{-1} . The corresponding capacity fading rates was only $2.7 \times 10^{-3}\%$ per cycle. Meanwhile, the coulombic efficiencies approach 100% even at the identical charge and discharge rates.

Fig. 9 shows the cyclic voltammograms of cells using $\text{Li}_4\text{Ti}_5\text{O}_{12}$ anode calcined at 750 $^{\circ}\text{C}$ for 5 h at the scanning rate of 0.5 mV s $^{-1}$ between 1.0 and 3.0 V. As shown in Fig. 9, only a pair of reversible redox peaks was observed. On the other hand, the redox peaks were sharp and show well-defined splitting. These results confirm

that the nano- $\text{Li}_4\text{Ti}_5\text{O}_{12}$ is very pure, in accordance with the XRD results. For the first discharge and charge cycle, the curve shows one cathodic peak located at $\sim 1.51 \text{ V}$ (vs. Li) correspond to the voltage platform of the first discharge process in which Li intercalated into the $\text{Li}_4\text{Ti}_5\text{O}_{12}$ anode. And there is also another anodic peak at $\sim 1.65 \text{ V}$ correspond to the voltage platform of the first charge process in which Li deintercalated from the anode. Meanwhile, the value of the symmetrical redox peaks after 50 cycles changed to $\sim 1.52 \text{ V}$ and $\sim 1.64 \text{ V}$, respectively. The potential difference between anodic and cathodic peaks was reduced from 140 mV to 120 mV. Such difference may be caused by the deposited time or electrochemical polarization. As compared to the first and fiftieth cycles, it was found that the first anodic peak shows the larger peak area than the following cycle. It is believed that irreversible capacity of the $\text{Li}_4\text{Ti}_5\text{O}_{12}$ electrode gradually reduces with the increase of the cycle numbers, and then the balance value of reversible capacity is achieved. The above result can be proven by the symmetry degree of the redox peaks in Fig. 9.

Fig. 10A shows the EIS curves of the sample in the frequency range of 100 kHz to 0.1 Hz. It is well known that the high-frequency

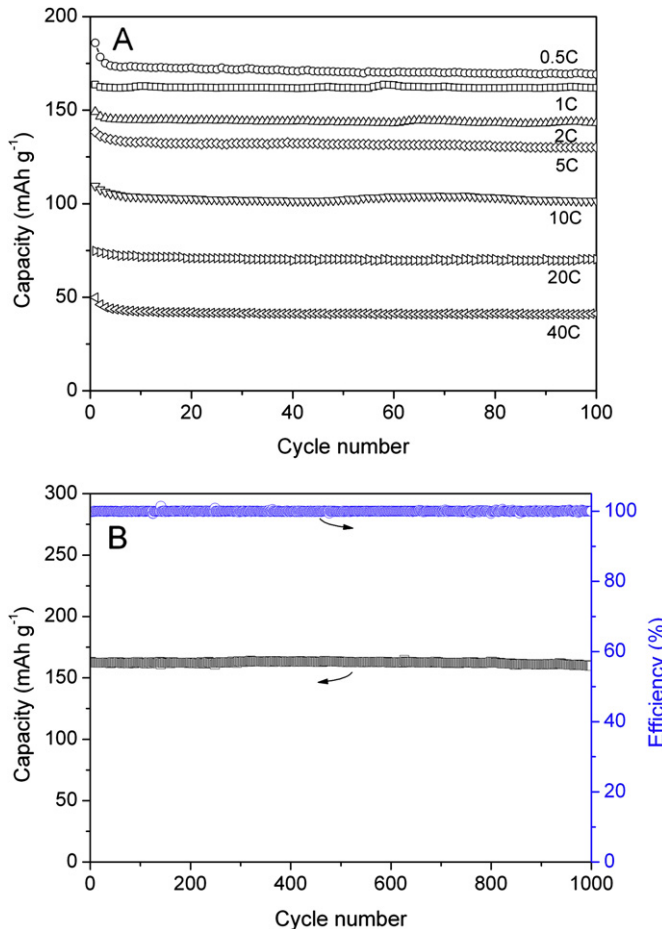


Fig. 8. Variation of the discharge capacities of the 750 °C for 5 h calcined $\text{Li}_4\text{Ti}_5\text{O}_{12}$ with the cycle voltage from 1 to 3 V at (A) different discharge rates between 0.5C and 40C; (B) 1C, the right ordinate is coulombic efficiency.

semicircle is related to the ohmic resistance; the high-to-medium frequency intercept is attributed to the contact resistance, polarization resistance, charge transfer resistance and corresponding capacitances; and the oblique line at the lower frequency range indicates the Warburg impedance of long-range Li-ion diffusion

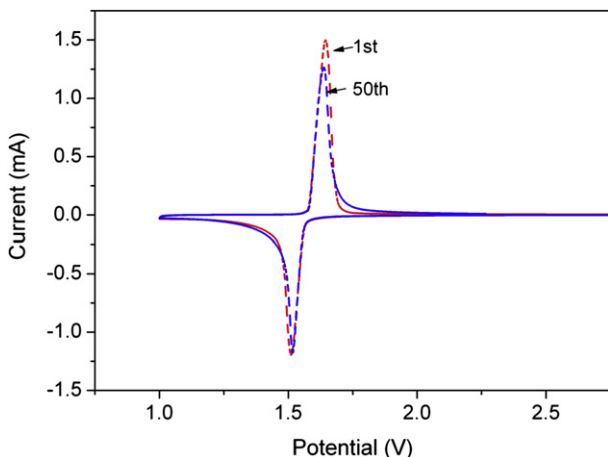


Fig. 9. Cyclic voltammograms of cells using the 750 °C for 5 h calcined $\text{Li}_4\text{Ti}_5\text{O}_{12}$ at the scanning rate of 0.5 mV s⁻¹.

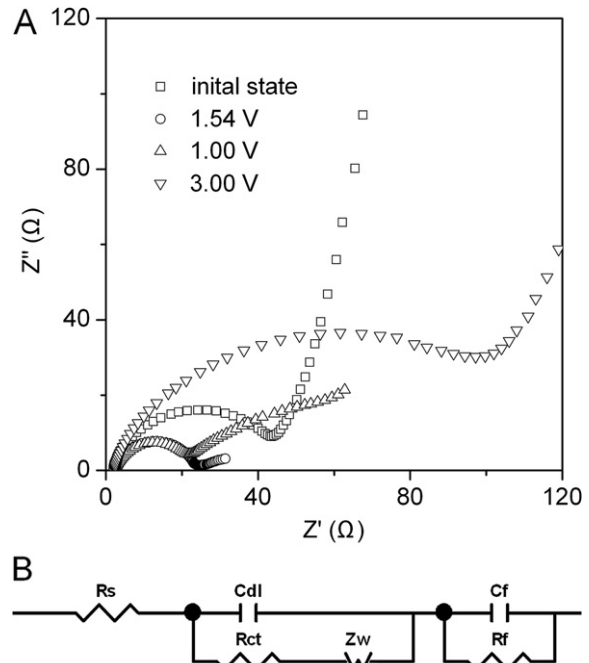


Fig. 10. (A) Impedance spectra of the half cell with the 750 °C for 5 h calcined $\text{Li}_4\text{Ti}_5\text{O}_{12}$ as anode, at the state of the original, the charging, the first totally discharged and charged at 1C rate. (B) Equivalent circuit for the Fig. 10A.

Table 2

The impedance parameters of the $\text{Li}_4\text{Ti}_5\text{O}_{12}$ electrodes derived using the equivalent circuit model (at discharging state of 1.54 V).

Temperature (°C)	Voltage (V)	R_s (Ω)	R_{ct} (Ω)
25	Initial state (2.7)	2.0	30.4
	1.00	2.3	15.6
	1.54	2.2	18.1
	3.00	2.4	85.9

through the $\text{Li}_4\text{Ti}_5\text{O}_{12}$ electrode [46]. In Fig. 10B, the experimental results could be fitted well with the proposed equivalent circuit. In the equivalent circuit, R_s is attributed to the ohmic resistance of the electrolyte; R_{ct} indicates the charge transfer resistance at the active material interface; R_f is the polarization resistance; C_{dl} represents the double-layer capacitance, and C_f is the surface capacitance. Z_w means the Warburg impedance caused by a semi-infinite diffusion of Li^+ in the electrode. As can be seen from Table 2 that R_{ct} increased obviously from the fully discharge state to charge state. It confirms that the intercalation/extraction process at the electrolyte/electrode interface is gradually improved after the charging.

4. Conclusions

Nano- $\text{Li}_4\text{Ti}_5\text{O}_{12}$ material has been successfully synthesized by a novel EDTA–CA sol–gel method. The products, which calcined at 750 and 800 °C with the ratio of Li/Ti was 4.2:5, have pure phase and good crystallinity. The $\text{Li}_4\text{Ti}_5\text{O}_{12}$ powders show the smallest particle size of 150–400 nm and porous appearance while the precursor was calcined at 750 °C for 5 h. The gases, which were produced from the bi-components chelating agent during the combustion process, could effectively prevent the aggregation and subsequent grain growth of the nanoparticle. The electrochemical performance of this $\text{Li}_4\text{Ti}_5\text{O}_{12}$ exhibits excellent discharge capacity of 164 and 108 mAh g⁻¹ at 1C and 10C discharge rate, respectively,

even with fairly stable cycling performance at 40C. After 1000 cycles, the discharge capacity was still as high as 160 mAh g⁻¹ due to the activity material with good crystallinity and phase purity. The cyclic voltammogram measurement also indicates that the electrochemical reaction of Li₄Ti₅O₁₂ has excellent reversibility and cycling performance. Thus, the EDTA–CA sol–gel method is a promising technique to prepare nano-Li₄Ti₅O₁₂ material with better performance.

Acknowledgments

This work was supported by the National Natural Science Foundation of China under contract No. 21171116 and the International Science & Technology Cooperation Program of China under contract No. 2012DFG11660. The first author would also like to thank Dr. Ye Lin at University of South Carolina for offering help with discussion and revision.

References

- [1] K. Smith, C. Wang, J. Power Sources 160 (2006) 662–673.
- [2] M. Armand, J.M. Tarascon, Nature 451 (2008) 652–657.
- [3] C. Samaras, K. Meisterling, Environ. Sci. Technol. 42 (2008) 3170–3176.
- [4] J.B. Goodenough, Y. Kim, Chem. Mater. 22 (2010) 587–603.
- [5] H.M. Wu, I. Belharouak, A. Abouimrane, Y.K. Sun, K. Amine, J. Power Sources 195 (2010) 2909–2913.
- [6] M. Winter, J.O. Besenhard, M.E. Spahr, P. Novak, Adv. Mater. 10 (1998) 725–763.
- [7] R.M. Dell, Solid State Ionics 134 (2000) 139–158.
- [8] D. Aurbach, E. Zinigrad, Y. Cohen, H. Teller, Solid State Ionics 148 (2002) 405–416.
- [9] A.S. Aricò, P. Bruce, B. Scrosati, J.M. Tarascon, W. Van Schalkwijk, Nat. Mater. 4 (2005) 366–377.
- [10] P.G. Bruce, B. Scrosati, J.M. Tarascon, Angew. Chem. Int. Ed. 47 (2008) 2930–2946.
- [11] T. Ohzuku, A. Ueda, N. Yamamoto, J. Electrochem. Soc. 142 (1995) 1431–1435.
- [12] K. Zaghib, M. Simoneau, M. Armand, M. Gauthier, J. Power Sources 81–82 (1999) 300–305.
- [13] A. Du Pasquier, A. Laforgue, P. Simon, J. Power Sources 125 (2004) 95–102.
- [14] K. Kanamura, T. Chiba, K. Dokko, J. Eur. Ceram. Soc. 26 (2006) 577–581.
- [15] T. Yuan, X. Yu, R. Cai, Y. Zhou, Z. Shao, J. Power Sources 195 (2010) 4997–5004.
- [16] L. Zhao, Y. Hu, H. Li, Z. Wang, L. Chen, Adv. Mater. 23 (2011) 1385–1388.
- [17] G.N. Zhu, Y.G. Wang, Y.Y. Xia, Energy Environ. Sci. 5 (2012) 6652.
- [18] Y.H. Rho, K. Kanamura, J. Solid State Chem. 177 (2004) 2094–2100.
- [19] C.Y. Ouyang, Z.Y. Zhong, M.S. Lei, Electrochim. Commun. 9 (2007) 1107–1112.
- [20] M. Kalbáč, M. Zukalová, L. Kavan, J. Electrochem. Soc. 8 (2003) 2–6.
- [21] W.J.H. Borghols, M. Wagemaker, U. Lafont, E.M. Kelder, F.M. Mulder, J. Am. Chem. Soc. 131 (2009) 17786–17792.
- [22] N. Zhang, Z. Liu, T. Yang, C. Liao, Z. Wang, K. Sun, Electrochim. Commun. 13 (2011) 654–656.
- [23] S. Huang, Z. Wen, X. Zhu, X. Yang, J. Electrochim. Soc. 152 (2005) A1301–A1305.
- [24] Y. Wang, Y. Hao, Q. Lai, J. Lu, Y. Chen, X. Ji, Ionics 14 (2007) 85–88.
- [25] A. Sivashanmugam, S. Gopukumar, R. Thirunakaran, C. Nithya, S. Prema, Mater. Res. Bull. 46 (2011) 492–500.
- [26] C. Li, Q. Li, L. Chen, T. Wang, ACS Appl. Mater. Inter. 4 (2012) 1233–1238.
- [27] Z. Liu, N. Zhang, Z. Wang, K. Sun, J. Power Sources 205 (2012) 479–482.
- [28] Y. Wang, H. Liu, K. Wang, H. Eiji, Y. Wang, H. Zhou, J. Mater. Chem. 19 (2009) 6789–6795.
- [29] H. Jung, J. Kim, B. Scrosati, Y. Sun, J. Power Sources 196 (2011) 7763–7766.
- [30] L. Cheng, J. Yan, G.N. Zhu, J.Y. Luo, C.X. Wang, Y.Y. Xia, J. Mater. Chem. 20 (2010) 595–602.
- [31] I. Belharouak, G.M. Koenig, K. Amine, J. Power Sources 196 (2011) 10344–10350.
- [32] P. Kubiak, A. Garcia, M. Worms, L. Aldon, J. Olivier Fourcade, P.E. Lippens, J.C. Jumas, J. Power Sources 119–121 (2003) 626–630.
- [33] K. Kanamura, N. Akutagawa, K. Dokko, J. Power Sources 146 (2005) 86–89.
- [34] B. Zhang, Z. Huang, S.W. Oh, J.K. Kim, J. Power Sources 196 (2011) 10692–10697.
- [35] D. Dambournet, I. Belharouak, J. Ma, K. Amine, J. Power Sources 196 (2011) 2871–2874.
- [36] S. Huang, Z. Wen, Z. Gu, X. Zhu, Electrochim. Acta 50 (2005) 4057–4062.
- [37] Y. Qi, Y. Huang, D. Jia, S. Bao, Z.P. Guo, Electrochim. Acta 54 (2009) 4772–4776.
- [38] S. Huang, Z. Wen, X. Zhu, Z. Gu, Electrochim. Commun. 6 (2004) 1093–1097.
- [39] M. Ganeshan, M.V.T. Dhananjayan, K.B. Sarangapani, N.G. Renganathan, J. Electroceram. 18 (2007) 329–337.
- [40] Z. Lin, X. Hu, Y. Huai, L. Liu, Z. Deng, J. Suo, Solid State Ionics 181 (2010) 412–415.
- [41] J. Wang, X. Liu, H. Yang, X. Shen, J. Alloys Compd 509 (2011) 712–718.
- [42] W. Zhou, Z. Shao, W. Jin, J. Alloys Compd 426 (2006) 368–374.
- [43] C. Zhang, Y. Zheng, R. Ran, Z. Shao, W. Jin, N. Xu, J. Ahn, J. Power Sources 179 (2008) 640–648.
- [44] Y. Hao, Q. Lai, D. Liu, Z. Xu, X. Ji, Mater. Chem. Phys. 94 (2005) 382–387.
- [45] T. Yuan, R. Cai, Z. Shao, J. Phy. Chem. C 115 (2011) 4943–4952.
- [46] C. Ho, I.D. Raistrick, R.A. Huggins, J. Electrochim. Soc. 127 (1980) 343–350.